Preface

Many-particle physics is at work whenever we delve into the rich phenomenology of the real world, or into laboratory experiments. Nevertheless, our physical description of nature is mostly built upon single-particle theories. For instance, Kepler's laws provide a basic understanding of our solar system, many features of the periodic table can be understood from the solution of a single hydrogen atom, and even complicated microprocessors with an unbearable number of electrons floating through millions of transistors can be developed based on the effective single-particle models of semiconductor physics. These approaches are successful because quite often interactions affect physical systems in a perturbative way. Classical perturbation theory yields corrections to a planet's orbit due to other planets, quantum chemistry relies on various approximation schemes to deal with complicated atoms and small molecules, and solid state theory uses weakly interacting quasiparticles as elementary excitations. This fortunate situation changes, however, when we try to understand more complex or strongly interacting systems, or when we try to explore the nature of matter itself. Condensates of cold bosonic atoms, for example, show subtle many-particle effects, strongly correlated fermions may give rise to high-temperature superconductivity, and the way quarks build up elementary particles (hadronization) is a highly non-trivial few-body problem. Another example are quantum computers, which many scientist envision as a replacement for our present-day microprocessors, and which exploit the entanglement property of quantum many-particle states. Last but not least, we mention the complexity of fusion plasmas, which some day may help feeding our ever-growing hunger for new energy resources. Unfortunately, even the most sophisticated analytical approaches largely fail to describe such systems. Hence, at present, unbiased numerical investigations provide the most reliable tool to address these problems. This is the point where the expert use of large-scale computers comes into play.

The increasing importance of computational many-particle physics calls for a comprehensive introduction into this rapidly developing field suitable for graduate students and young researchers. Therefore, we decided to organize a summer school on "Computational Many-Particle Physics" in September 2006, during the 550th anniversary of the University Greifswald. Generously sponsored by the Wilhelm and Else Heraeus Foundation and hosted by the Max-Planck-Institute for Plasma Physics and the Institute for Physics, we brought together more than 40 students and 20 distinguished scientists working on such diverse fields as fusion plasmas,

statistical physics, solid state theory and high performance computing. The present Lecture Notes summarize and extend the material showcased over a 2-week period of tightly scheduled tutorials, seminars and exercises. The emphasis is on a very pedagogical and systematic introduction to various numerical concepts and techniques, with the hope that the reader may quickly start to program himself. The spectrum of the numerical methods presented is very broad, covering classical as well as quantum few- and many-particle systems. The trade-off between the number of particles, the complexity of the underlying microscopic models and the importance of the interactions determine the choice of the appropriate numerical approach. Therefore, we arranged the book along the algorithms and techniques employed, rather than on the physics applications, which we think is more natural for a book on numerical methods.

We start with methods for classical many-particle systems. Here, molecular dynamics approaches trace the motion of individual particles, kinetic approaches work with the distribution functions of particles and momenta, while hybrid approaches combine both concepts. A prominent example is the particle-in-cell method typically applied to model plasmas, where the time evolution of distribution functions is approximated by the dynamics of pseudo-particles, representing thousands or millions of real particles. Of course, at a certain length scale the quantum nature of the particles becomes important. As an attempt to close the gap between classical and quantum systems, we outline a number of semi-classical (Wigner-function, Boltzmann- and Vlasov-equation based) approaches, which in particular address transport properties. The concept of Monte Carlo sampling is equally important for classical, statistical and quantum physical problems. The corresponding chapters therefore account for a substantial part of the book and introduce the major stochastic approaches in application to very different physical situations. Focussing on solids and their properties, we continue with ab initio approaches to the electronic structure problem, where band structure effects are taken into account with full detail, but Coulomb interactions and the resulting correlations are treated approximately. Dynamical mean field theories and cluster approaches aim at improving the description of correlations and bridge the gap to an exact numerical treatment of basic microscopic models. Exact diagonalization of finite systems gives access to their ground-state, spectral and thermodynamic properties. Since these methods work with the full many-particle Hamiltonian, the study of a decent number of particles or larger system sizes is a challenging task, and there is a strong demand to circumvent these limitations. Along this line the density matrix renormalization group represents a clever technique to restrict the many-particle Hilbert space to the physically most important subset. Finally, all the discussed methods heavily rely on the use of powerful computers, and the book would be incomplete without two detailed chapters on parallel programming and optimization techniques for high performance computing.

Of course, the preparation of such a comprehensive book would have been impossible without support from many colleagues and sponsors. First of all, we thank the lecturers and authors for their engagement, enthusiasm and patience. We are

Greifswald,   *Holger Fehske*
July 2007   *Ralf Schneider*
                                                                 Alexander Weiße

2 Wigner Function Quantum Molecular Dynamics

V. S. Filinov[1,2], M. Bonitz[2], A. Filinov[2], and V. O. Golubnychiy[2]

[1] Institute for High-Energy Density, Russian Academy of Sciences, Moscow
127412, Russia

[2] Institut für Theoretische Physik und Astrophysik, Christian-Albrechts-Universität,
24098 Kiel, Germany

Classical molecular dynamics (MD) is a well established and powerful tool in various fields of science, e.g. chemistry, plasma physics, cluster physics and condensed matter physics. Objects of investigation are few-body systems and many-body systems as well. The broadness and level of sophistication of this technique is documented in many monographs and reviews, see for example [1, 2]. Here we discuss the extension of MD to quantum systems (QMD). There have been many attempts in this direction which differ from each other, depending on the type of system under consideration. One variety of QMD has been developed for condensed matter systems. This approach is reviewed e.g. in [3] and will not be discussed here. In this contribution we deal with unbound electrons as they occur in gases, fluids or plasmas. Here, a quite successful strategy is to replace classical point particles by wave packets [3, 4, 5, 6]. This method, however, struggles with problems related to the dispersion of such a wave packet and difficulties to properly describe strong electron-ion interaction and bound-state formation. We try to avoid these restrictions by an alternative approach: We start the discussion of quantum dynamics by a general consideration of quantum distribution functions.

2.1 Quantum Distribution Functions

There exists a variety of different representations of quantum mechanics including the so-called *Wigner representation* which involves a class of functions depending on coordinates and momenta. In the classical limit, the Wigner distribution function f_W turns into the phase space distribution f known from classical statistical mechanics. In contrast to f, the Wigner function may be non-positive as a consequence of the coordinate-momentum (Heisenberg) uncertainty. This will lead to a modification of the particle trajectories which is discussed in Sect. 2.3. An important property of the distribution functions is that they can be used to compute the expectation value of an arbitrary physical observable $\langle A \rangle$, defined by the operator $\widehat{A}(\widehat{p}, \widehat{q})$ [7]

$$\langle A \rangle(t) = \int dp\, dq\, A_W(p, q)\, f_W(p, q, t)\,, \qquad 1 = \int dp\, dq\, f_W(q, p, t)\,, \quad (2.1)$$

where $A_W(p, q)$ is a scalar function. For simplicity we considered the one-dimensional (1D) case; the generalization to higher dimensions and N particles

is straightforward by re-defining the coordinate and momentum as vectors, $q = \{q_1, \ldots, q_N\}$, $p = \{p_1, \ldots, p_N\}$. f_W is defined via the nonequilibrium N-particle density operator $\hat{\rho}$ in coordinate representation (i.e. the density matrix),

$$f_W(p, q, t) = \frac{1}{2\pi\hbar} \int d\nu \left\langle q + \frac{\nu}{2} |\hat{\rho}| q - \frac{\nu}{2} \right\rangle e^{-i\nu p} , \qquad (2.2)$$

and $A_W(p, q)$ is analogously defined from the coordinate representation of $\hat{A}$.

We now consider the time evolution of the wave function under the influence of a general Hamiltonian of the form

$$\hat{H} = \sum_{j=1}^{N} \frac{\hat{p}_i^2}{2m} + \sum_{i=1}^{N} \widetilde{V}(q_i) + \sum_{i<j} V(q_i, q_j) , \qquad (2.3)$$

where $\widetilde{V}(q_i)$ and $V(q_i, q_j)$ denote an external and an interaction potential, respectively. The equation of motion for f_W has the form [8, 7] (see also Sect. 2.3)

$$\frac{\partial f_W}{\partial t} + \frac{p}{m} \cdot \nabla_q f_W = \int_{-\infty}^{\infty} ds \, f_W \, (p - s, q, t) \, \widetilde{\omega} \, (s, q, t) , \qquad (2.4)$$

where the function

$$\widetilde{\omega} \, (s, q, t) = \frac{2}{\pi\hbar^2} \int dq' V \, (q - q', t) \sin \left(\frac{2sq'}{\hbar} \right) \qquad (2.5)$$

takes into account the non-local contribution of the potential energy in the quantum case. Equivalently, expanding the integral around $q' = 0$, (2.4) can be rewritten by an infinite sum of local potential terms

$$\frac{\partial f_W}{\partial t} + \frac{p}{m} \frac{\partial f_W}{\partial q} = \sum_{n=0}^{\infty} \frac{(\hbar/(2i))^{2n}}{(2n+1)!} \left(\frac{\partial^{2n+1} V}{\partial q^{2n+1}}, \frac{\partial^{2n+1} f_W}{\partial p^{2n+1}} \right) , \qquad (2.6)$$

where $(\partial^{2n+1} V/\partial q^{2n+1}, \partial^{2n+1} f_W/\partial p^{2n+1})$ denotes the scalar product of two vectors which for an N-particle system contain $3N$ components.

If the potential does not contain terms higher than second order in q, i.e. $\partial^n V/\partial q^n|_{n\geq 3} = 0$, (2.6) reduces to the classical Liouville equation for the distribution function f:

$$\frac{\partial f}{\partial t} + \frac{p}{m} \frac{\partial f}{\partial q} = \frac{\partial V}{\partial q} \frac{\partial f}{\partial p} . \qquad (2.7)$$

The Wigner function must satisfy a number of conditions [9], therefore, the initial function $f_W(q, p, 0)$ cannot be chosen arbitrarily. Even if $f_W(q, p, t)$ satisfies the classical equation (2.7) it nevertheless describes the evolution of a quantum distribution because a properly chosen initial function $f_W(q, p, 0)$ contains, in general, all

powers of $\hbar$. In particular, the uncertainty principle holds for averages of operators calculated with $f_W(q, p, 0)$ and $f_W(q, p, t)$.

One can rewrite (2.6) in a form analogous to the classical Liouville equation (2.7) by replacing V by a new effective potential V_{eff} defined as

$$\frac{\partial V_{\text{eff}}}{\partial q} \frac{\partial f_W}{\partial p} = \frac{\partial V}{\partial q} \frac{\partial f_W}{\partial p} - \frac{\hbar^2}{24} \frac{\partial^3 V}{\partial q^3} \frac{\partial^3 f_W}{\partial p^3} + \cdots . \tag{2.8}$$

Equation (2.7) can be efficiently solved with the *method of characteristics*, see e.g. [10]. This is the basis of our QMD approach where an ensemble of classical (Wigner) trajectories is used to solve (numerically) the quantum Wigner-Liouville equation (2.4) which will be discussed in Sect. 2.3. The time-dependence of the trajectories is given by the classical equations of motion

$$\frac{\partial q}{\partial t} = \frac{p}{m} , \qquad \frac{\partial p}{\partial t} = -\frac{\partial V_{\text{eff}}(p, q, t)}{\partial q} . \tag{2.9}$$

Of course, a direct solution of (2.9) with the definition (2.8) is only useful if the series is rapidly converging and there is only a small number of non-zero terms.

Clearly there is a principle difficulty with this approach if the series of terms with the potential derivatives is not converging. This is the case, e.g., for a Coulomb potential (at zero distance). There are at least three solutions to this problem. The first one is to solve the Wigner-Liouville equation by Monte Carlo (MC) techniques [11, 12, 13, 14], which is discussed below in Sect. 2.3. The second one is to replace the original potential on the r.h.s. of (2.8) by some model potential having a finite number of nonzero derivatives, see e.g. [15]. The third approach is to perform a suitable average of V_{eff}, e.g. over a thermal ensemble of particles. This has been done both for external potentials and also for two particle interaction. The use of an effective quantum pair potential in classical MD is discussed in Chap. 1.

2.2 Semiclassical Molecular Dynamics

2.2.1 Quantum Pair Potentials

In order to obtain an effective pair potential which is finite at zero interparticle distance, we consider (2.4) for two particles. Assuming further thermodynamic equilibrium with a given temperature $k_B T = 1/\beta$, spatial homogeneity and neglecting three-particle correlations, one can solve for the two-particle Wigner function $f_{W,12} = F_{12}^{\text{eq}}(r_1, p_1, r_2, p_2, \beta) \approx F_{12}^{\text{eq}}(r_1 - r_2, p_1, p_2, \beta)$.

This is now rewritten as in the canonical case [7], $F_{12}^{\text{eq}}(r_1 - r_2, p_1, p_2, \beta) \equiv F_1^{\text{eq}}(p_1, \beta) F_2^{\text{eq}}(p_2, \beta) \exp(-\beta V_{12}^{\text{qp}})$, which defines the desired quantum pair potential V_{12}^{qp}.

The first solution for V_{12}^{qp} was found by Kelbg in the limit of weak coupling [16, 17, 18]. It has the form of (2.10) with $\gamma_{ij} \to 1$, for details and references see [10, 19]. The Kelbg potential, or slightly modified versions, is widely used in numerical simulations of dense plasmas [4, 5, 20, 21, 22]. It is finite at zero distance

which correctly captures basic quantum diffraction effects preventing any divergence. However, the absolute value at $r = 0$ is incorrect which has lead to the derivation of further improved potentials, see [10, 19, 23] and references therein. Here we use the *improved Kelbg potential* (IKP),

$$\Phi\left(r_{ij}, \beta\right) = \frac{q_i q_j}{r_{ij}} \left\{ 1 - \mathrm{e}^{-r_{ij}^2/\lambda_{ij}^2} + \sqrt{\pi} \frac{r_{ij}}{\lambda_{ij}\gamma_{ij}} \left(1 - \mathrm{erf}\left[\gamma_{ij} \frac{r_{ij}}{\lambda_{ij}} \right] \right) \right\} , \quad (2.10)$$

where $r_{ij} = |\boldsymbol{r}_{ij}|$, $x_{ij} = r_{ij}/\lambda_{ij}$, $\lambda_{ij}^2 = \hbar^2\beta/(2\mu_{ij})$ and $\mu_{ij}^{-1} = m_i^{-1} + m_j^{-1}$, which contains additional free parameters γ_{ij} that can be obtained from a fit to the exact solution of the two-particle problem [19].

2.2.2 Molecular Dynamics Simulations

We have performed extensive MD simulations of dense partially ionized hydrogen in thermodynamic equilibrium using different IKP for electrons with different spin projections. To properly account for the long-range character of the potentials, we used periodic boundary conditions with the standard Ewald procedure, see Chap. 1. The number of electrons and protons was $N = 200$. For our MD simulations we use standard Runge-Kutta or Verlet algorithms (see Chap. 1) to solve Newton's equations (2.9), where V_{eff} is replaced by the IKP. Because of the temperature dependence of the IKP we applied a temperature scaling at every time step for all components separately (for protons and two sorts of electrons) to guarantee a constant temperature of all components in our equilibrium simulations. In each simulation the system was equilibrated for at least 10^4 MD steps, only after this the observables have been computed.

In Fig. 2.1 we show the internal energy per atom as a function of temperature for two densities and compare it to path integral Monte Carlo (PIMC) results [19, 24]. The density is given by the Brueckner parameter $r_s = \bar{r}/a_B$, where $\bar{r}$ is the average interparticle distance and a_B denotes the Bohr radius. For high temperatures and weak coupling, $\Gamma = e^2/(\bar{r}k_{\mathrm{B}}T) < 1$ for the fully ionized plasma, the two simulations coincide within the limits of statistical errors. If we use the original Kelbg potential, at temperatures below $300\,000\,\mathrm{K}$ (approximately two times the binding energy), the MD results start to strongly deviate from the PIMC results. In contrast the IKP fully agrees with the PIMC data even at temperatures far below the hydrogen binding energy (1 Ry), where the plasma is dominated by atoms, which is a remarkable extension of semi-classical MD into the theoretically very difficult regime of moderate coupling, moderate degeneracy and partial ionization.

Interestingly, even bound states can be analyzed in our simulations by following the electron trajectories. At $T < 1$ Ry, we observe an increasing number of electrons undergoing strong deflection (large-angle scattering) on protons and eventually performing quasi-bound trajectories. Most of these electrons remain bound only for a few classical orbits and then leave the proton again. Averaged over a long time, our simulations are able to reveal the degree of ionization of the plasma. For temperatures below approximately $50\,000\,\mathrm{K}$, which is close to the binding energy of hydrogen molecules, the simulations cannot be applied. Although we clearly observe
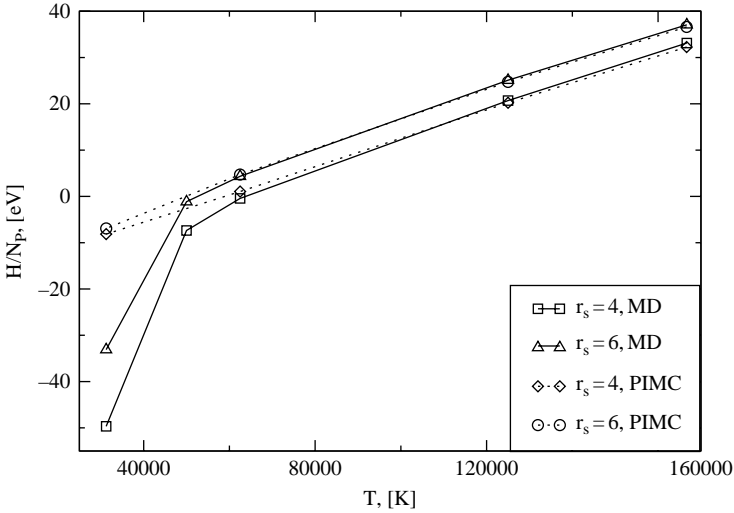
Fig. 2.1. Internal energy per hydrogen atom at $r_s = 4$ and $r_s = 6$ versus temperature, MD results are compared to restricted PIMC simulations [19, 24]

molecule formation (see below), there also appear clusters of several molecules which is unphysical under the present conditions and is caused by the approximate two-particle treatment of quantum effects in the IKP. This turns out to be the reason for the too small energy at low temperatures (see Fig. 2.1).

Let us now turn to a more detailed analysis of the spatial configuration of the particles. In Fig. 2.2 the pair distribution functions of all particle species with the same charge are plotted at two densities. Consider first the case of $T = 125\,000$ K (upper panels). For both densities all functions agree qualitatively showing a depletion at zero distance due to Coulomb repulsion. Besides, there are differences which arise from the spin properties. Electrons with the same spin show a *Coulomb hole* around $r = 0$ which is broader than the one of the protons due to the Pauli principle with additional repulsion of electrons with the same spin projection. This trend is reversed at low temperatures (see middle panel), which is due to the formation of hydrogen atoms and molecules. In this case, electrons, i.e., their classical trajectories, are spread out around the protons giving rise to an increased probability of close encounters of two electrons belonging to different atoms compared to two protons.

Now, let us compare electrons with parallel and electrons with anti-parallel spins. In all cases, we observe a significantly increased probability to find two electrons with opposite spin at distances below one Bohr radius, which is due to the missing Pauli repulsion. This trend increases when the temperature is lowered because of increasing quantum effects. Before analyzing the lowest temperature in Fig. 2.2, let us consider the electron-proton (e-p) distributions. Multiplying these functions by r^2 gives essentially the radial probability density $W_{ep}(r) = r^2 g_{ep}(r)$,
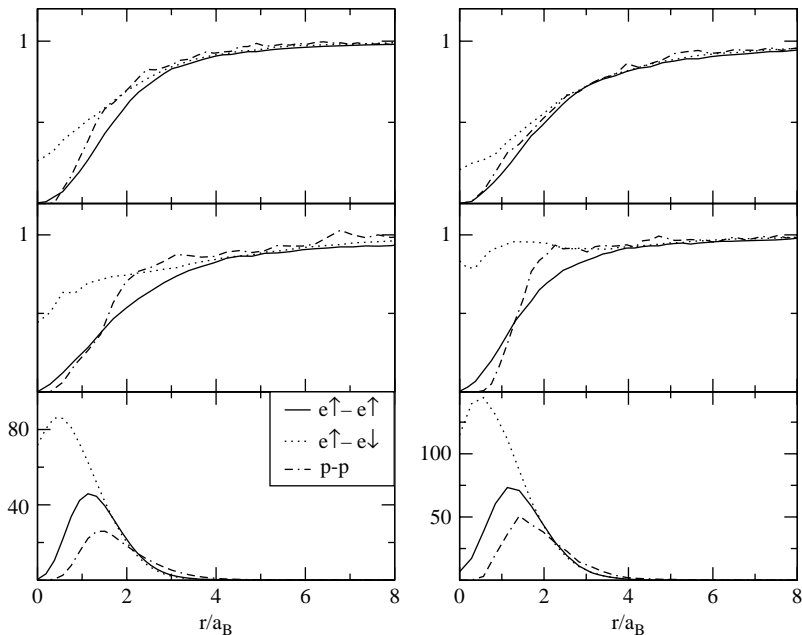
Fig. 2.2. Electron-electron (e-e) and proton-proton (p-p) pair distribution functions for a correlated hydrogen plasma with $r_s = 4$ (**left row**) and $r_s = 6$ (**right row**) for $T = 125\,000$ K, $61\,250$ K and $31\,250$ K (**from top to bottom**) [19]

which is plotted in Fig. 2.3. At low temperatures this function converges to the ground state probability density of the hydrogen atom $W_{ep}(r) = r^2|\psi|^2_{1s}(r)$ influenced by the surrounding plasma. Here, lowering of the temperature leads towards the formation of a shoulder around $1.4a_B$ for $r_s = 4$ and $1.2a_B$ for $r_s = 6$ which is due to the formation of hydrogen atoms; this is confirmed by the corresponding quasi-bound electron trajectories. At this temperature, the observed most probable electron distance is slightly larger than one a_B as in the atom hydrogen ground state. Of course, classical MD cannot yield quantization of the bound electron motion, but it correctly reproduces (via averaging over the trajectories) the statistical properties of the atoms, such as the probability density averaged over the energy spectrum.

At 62 500 K and $r_s = 6$ (right middle part of Fig. 2.2) the simulations show a first weak signature of molecule formation – see the maximum of the p-p distribution function around $r = 2a_B$ and the maximum of the distribution function of electrons with anti-parallel spins around $r = 1.5a_B$. Upon further lowering of the temperature by a factor of two (lower panel of Fig. 2.2) the p-p functions exhibit a clear peak very close to $r = 1.4a_B$, the theoretical p-p separation in H_2. At the same time, also the e-e functions have a clear peak around $r = 0.5a_B$, the two electrons are concentrated between the protons. In contrast, in the case of parallel spins, no molecules are formed, the most probable electron distance is around $r = 1.2a_B$.
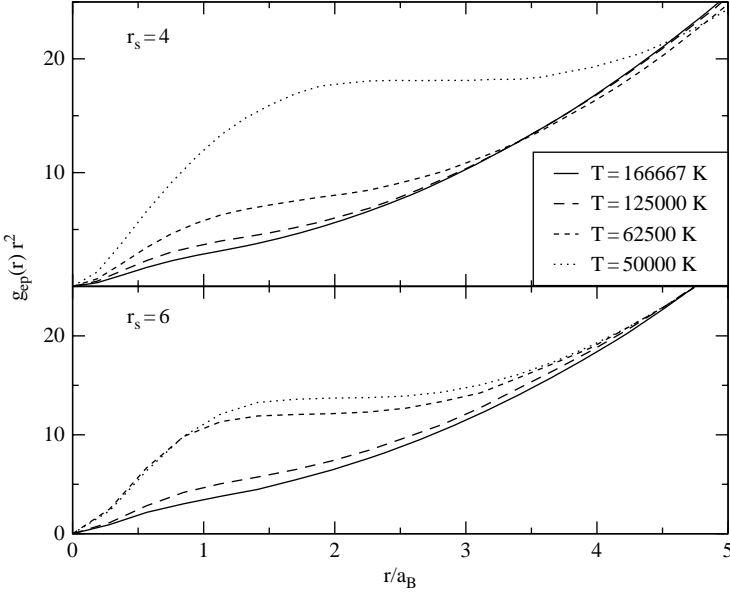
Fig. 2.3. Electron-proton (e-p) pair distribution functions multiplied by r^2 as function of e-p distance at $r_s = 4$ (**top**) and $r_s = 6$ (**bottom**) at four temperatures [19]

2.2.3 Molecular Dynamics Results for Dynamical Quantities

We now extend the analysis to the dynamical properties of a hydrogen plasma in equilibrium using the fluctuation-dissipation theorem. The time-dependent microscopic density of plasma species α is defined as

$$\rho^\alpha(\boldsymbol{r}, t) = \sum_{i=1}^{N_\alpha} \delta[\boldsymbol{r} - \boldsymbol{r}_i^\alpha(t)] , \tag{2.11}$$

with the Fourier components

$$\rho^\alpha(\boldsymbol{k}, t) = \sum_{i=1}^{N_\alpha} e^{i\boldsymbol{k}\cdot\boldsymbol{r}_i^\alpha(t)} , \tag{2.12}$$

where $\boldsymbol{r}_i^\alpha(t)$ denotes the trajectory of particle i obtained in the simulation. We now define the three partial density-density time correlation functions (DDCF) between sorts α and η as

$$A^{\alpha\eta}(\boldsymbol{k}, t) = \frac{1}{N_\alpha + N_\eta} \langle \rho^\alpha(\boldsymbol{k}, t)\rho^\eta(-\boldsymbol{k}, 0) \rangle , \tag{2.13}$$

where, due to isotropy, $\boldsymbol{k} = k$. Here $\langle \rho^\alpha(\boldsymbol{k}, t)\rho^\eta(-\boldsymbol{k}, 0) \rangle$ denotes averaging along the trajectories by shifting the time interval and keeping the difference equal to t.

Note also, that $A^{\alpha\eta}(\boldsymbol{k},t) = A^{\eta\alpha}(\boldsymbol{k},t)$ for all pairs α and η. In addition to the spin-resolved electron functions we can also consider the spin averaged correlation function $A(\boldsymbol{k},t) = A^{\uparrow\uparrow}(\boldsymbol{k},t) + A^{\downarrow\uparrow}(\boldsymbol{k},t)$.

We have performed a series of simulation runs of equilibrium fluctuations in hydrogen plasmas with coupling parameters Γ and electron degeneracy parameters $\chi_e = \rho\Lambda_e^3$ with the electron de Broglie wavelength $\Lambda_e = \hbar/\sqrt{2\pi m_e k_B T}$ ranging from zero (classical system) to one (quantum or degenerate system). The electron DDCF for $\Gamma = 1$ and $\chi_e = 1$ are plotted in Fig. 2.4 for four values of the dimensionless wavenumber $q = k\bar{r}$. The correlation functions ($\uparrow\uparrow$ and $\downarrow\uparrow$) have two characteristic features – a highly damped, high-frequency part and a weakly damped low-frequency tail. The latter originates from slow ionic motion whereas the high-frequency part is related to oscillations with frequencies close to the electron plasma frequency ω_{pl}. On the other hand, the time scale of the ion motion is determined by the ion plasma frequency $\omega_{pl}^i = \sqrt{4\pi\rho_i Z_i^2 e^2/m_i}$, the ratio of the two time scales is $\sqrt{m_i/m_e} \approx 43$. The slow proton oscillations are clearly seen in the proton DDCF, shown in Fig. 2.5. To resolve the proton oscillations the whole simulation (including the electron dynamics) has to extend over several proton plasma periods $T_p = 2\pi/\omega_{pl}^i$ thereby resolving the fast electronic motions as well, which sets the numerical limitation of the calculation.

The temporal Fourier transform of the DDCF yields another very important quantity – the dynamic structure factor, $S_{\alpha,\eta}(\omega,q)$, which allows one to analyze, e.g., the dispersion of the coupled electron and proton oscillations. Fig. 2.6 shows
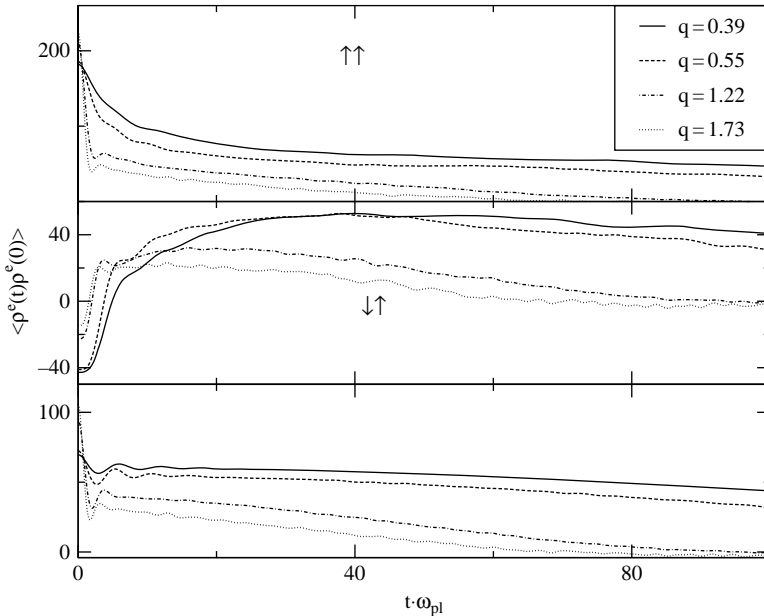

Fig. 2.4. Electron DDCF (2.13) multiplied by $(N_e^{\uparrow} + N_e^{\downarrow})$ for $\Gamma = 1$ and $\chi_e = 1$ for four wave vectors. **Upper (middle) panel**: Correlation functions for parallel (antiparallel) spins. **Bottom**: Spin-averaged function [25]
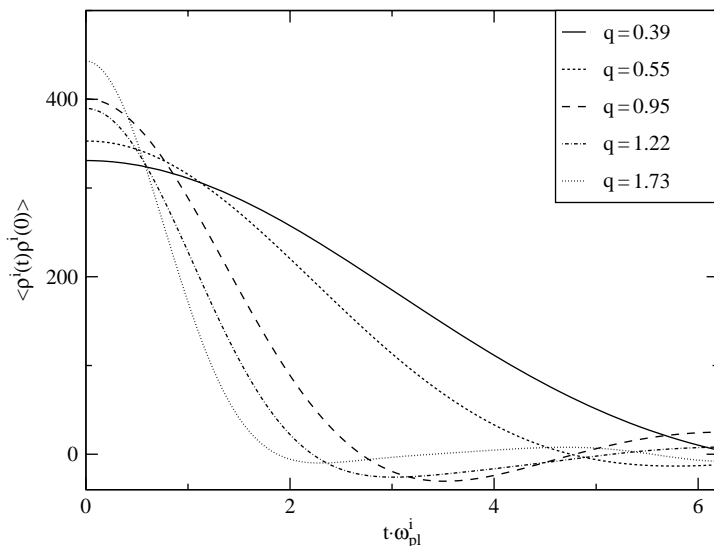
Fig. 2.5. Proton DDCF (2.13) for $\Gamma = 1$ and $\chi_e = 1$ for five wave vectors (in units of $1/\bar{r}$) [25]
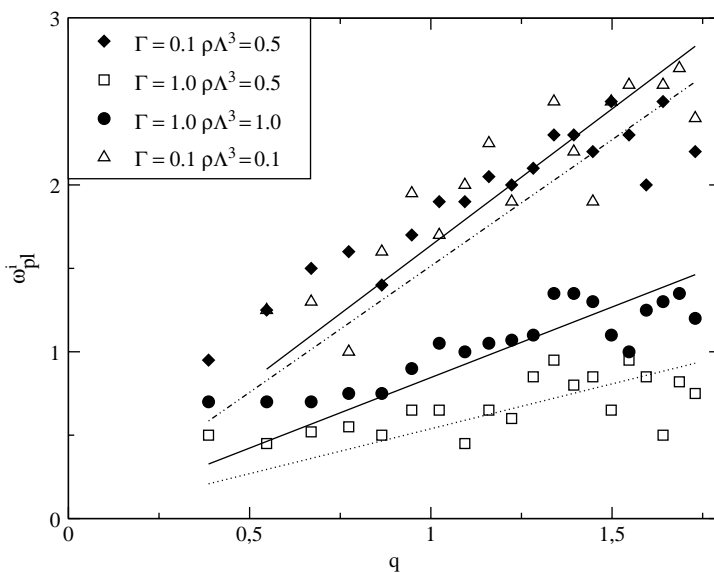

Fig. 2.6. Ion-acoustic wave dispersion in a dense hydrogen plasma. Lines correspond to weighted linear fits to the MD data (*symbols*). The scatter of the data is due to the limited particle number N and simulation time and can be systematically reduced. Also, smaller q-values require larger N [25]

dispersion results for the collective proton oscillations, for the electron modes see [22, 24], which follow from the peak positions of $S_{ii}(\omega, q)$. Fig. 2.6 shows the peak frequency versus wave number, i.e. the dispersion of longitudinal ion-acoustic waves, $\omega(q) = v_{\mathrm{MD}} q$, where v_{MD} denotes our MD result for the phase velocity. This can be compared to the familiar analytical expression for an ideal two-temperature ($T_e \gg T_i$) plasma $v_s = \sqrt{Z_i k_B T_e / m_i}$, where v_s is the ion sound velocity. We observe deviations of about 10% for weak degeneracy $\chi_e < 0.5$, and about 10% for large degeneracy $\chi_e \geq 1$, which are due to nonideality (correlations) and quantum effects, directly included in our simulations. For further details on this method see [6, 24, 25].

Thus semiclassical MD is a powerful approach to correlated quantum plasmas. Thermodynamic and dynamic properties are accurately computed if accurate quantum pair potentials, such as the IKP, are used.

2.3 Quantum Dynamics

Let us now discuss the method of Wigner trajectories in more detail. As we have seen, the Wigner function W (to avoid confusion, in this section we rename $f_{\mathrm{W}} \to W$) in (2.2) is the Fourier transform of the non-diagonal elements of the density matrix which, for a pure state, is $\rho\left(q + \frac{\nu}{2}, q - \frac{\nu}{2}\right) = \psi(q + \frac{\nu}{2}, t)\psi^*(q - \frac{\nu}{2}, t)$, where the $N-$particle wave functions satisfy the Schrödinger equation with an initial condition

$$i\hbar \frac{\partial \psi}{\partial t} = \widehat{H}\psi , \qquad \psi(t_0) = \psi^0(q) , \tag{2.14}$$

which contains the Hamiltonian (2.3); recall that q is a vector of dimension Nd. By taking the time derivative of W in (2.2) and substituting $\partial \psi / \partial t$ in the l.h.s of the Schrödinger equation we recover (2.4), after integrating by parts. For convenience, on both sides we add the contribution of the classical force, $\boldsymbol{F}(\boldsymbol{q}) = -\boldsymbol{\nabla}_q V(\boldsymbol{q})$, which leads to a new function ω which differs from $\widetilde{\omega}$ in (2.4) by an additional term, the last term in (2.16),

$$\frac{\partial W}{\partial t} + \frac{\boldsymbol{p}}{m} \cdot \boldsymbol{\nabla}_q W + \boldsymbol{F}(\boldsymbol{q}) \cdot \boldsymbol{\nabla}_p W = \int\limits_{-\infty}^{\infty} \mathrm{d}s \, W(p - s, q, t) \, \omega(s, q, t) , \tag{2.15}$$

$$\omega(s, q, t) = \frac{2}{(\pi\hbar^2)^{Nd}} \int \mathrm{d}q' V(q - q', t) \sin\left(\frac{2sq'}{\hbar}\right) + \boldsymbol{F}(q) \cdot \boldsymbol{\nabla}_s \delta(s) . \tag{2.16}$$

In the classical limit ($\hbar \to 0$), the r.h.s of (2.15) vanishes and we obtain the classical Liouville equation

$$\frac{\partial W}{\partial t} + \frac{\boldsymbol{p}}{m} \cdot \boldsymbol{\nabla}_q W + \boldsymbol{F}(\boldsymbol{q}) \cdot \boldsymbol{\nabla}_p W = 0 . \tag{2.17}$$

The solution of (2.17) is known and can be expressed by the Green function [9]

$$G(p, q, t; p_0, q_0, t_0) = \delta \left[p - \overline{p}(t; t_0, p_0, q_0) \right] \delta \left[q - \overline{q}(t; t_0, p_0, q_0) \right] , \qquad (2.18)$$

where $\overline{p}(\tau)$ and $\overline{q}(\tau)$ are the phase space trajectories of all particles, which are the solutions of Hamilton's equations with the initial conditions at $\tau = t_0 = 0$,

$$\frac{\mathrm{d}\overline{q}}{\mathrm{d}\tau} = \frac{\overline{p}(\tau)}{m}; \qquad \overline{q}(0) = q_0,$$

$$\frac{\mathrm{d}\overline{p}}{\mathrm{d}\tau} = \boldsymbol{F}(\overline{q}(\tau)); \qquad \overline{p}(0) = p_0. \qquad (2.19)$$

Using the Green function, the time-dependent solution of the classical Liouville equation takes the form

$$W(p, q, t) = \int \mathrm{d}p_0 \, \mathrm{d}q_0 \, G(p, q, t; p_0, q_0, 0) \, W_0(p_0, q_0) . \qquad (2.20)$$

With this result, it is now possible to construct a solution also for the quantum case. To this end we note that it is straightforward to convert (2.15) into an integral equation

$$W(p, q, t) = \int \mathrm{d}p_0 \, \mathrm{d}q_0 \, G(p, q, t; p_0, q_0, 0) \, W_0(p_0, q_0)$$

$$+ \int_0^t \mathrm{d}t_1 \int \mathrm{d}p_1 \, \mathrm{d}q_1 \, G(p, q, t; p_1, q_1, t_1)$$

$$\times \int_{-\infty}^{\infty} \mathrm{d}s_1 \, \omega(s_1, q_1, t_1) \, W(p_1 - s_1, q_1, t_1) , \qquad (2.21)$$

which is exact and can be solved efficiently by iteration [10, 11]. The idea is to replace the unknown function W under the integral in (2.21) by an approximation. The first approximation is obtained by solving (2.21) to lowest order, i.e. by neglecting the integral term completely. This gives the first order result for W which can again be substituted for W in the integral in (2.21) and so on. This way we can systematically derive improved approximations for W. The procedure leads to a series of terms of the following general form,

$$W(p, q, t) = W^{(0)}(p, q, t) + W^{(1)}(p, q, t) + \int_0^t \mathrm{d}t_1 \int \mathrm{d}1 \, G(p, q, t; 1, t_1)$$

$$\times \int_0^{t_1} \mathrm{d}t_2 \int \mathrm{d}2 \, G(p_1 - s_1, q_1, t_1; 2, t_2)$$

$$\times \int_{-\infty}^{\infty} \mathrm{d}s_2 \, \omega(s_2, q_2, t_2) \, W(p_2 - s_2, q_2, t_2) , \qquad (2.22)$$

where we have introduced the notations $n \equiv q_n, p_n$, $\mathrm{d}n \equiv \mathrm{d}q_n \mathrm{d}p_n$ and

$$W^{(0)}(p,q,t) = \int \mathrm{d}0 \; G(p,q,t;0,0) W_0(0) \;,$$

$$W^{(1)}(p,q,t) = \int_0^t \mathrm{d}t_1 \int_{-\infty}^{\infty} \mathrm{d}1 \; G(p,q,t;1,t_1) \int_{-\infty}^{\infty} \mathrm{d}s_1 \; \omega(s_1,q_1,t_1)$$

$$\times \int \mathrm{d}0 \; G(p_1 - s_1, q_1, t_1; 0, 0) W_0(0) \;. \qquad (2.23)$$

The terms $W^{(0)}$ and $W^{(1)}$ are the first of an infinite series. To shorten the notation, all higher order terms are again summed up giving rise to the last term in (2.22). Below we will give also the third term, $W^{(2)}$, but first we discuss the physical interpretation of each contribution.

$W^{(0)}(p,q,t)$, as it follows from the Green function $G(p,q,t;p_0,q_0,0)$, describes the propagation of the Wigner function along the classical characteristics, i.e., the solutions of Hamilton's equations (2.19) in the time interval $[0,t]$. It is worth mentioning, that this first term describes both classical and quantum effects, due to the fact that the initial Wigner function $W_0(p_0,q_0)$, in general, contains all powers of Planck's constant $\hbar$ contained in the initial state wave functions. These are quantum diffraction and spin effects, depending on the quality of the initial function.

The second and third terms on the r.h.s. of (2.22) describe additional quantum corrections to the time evolution of $W(p,q,t)$ arising from non-classical time propagation, in particular, the Heisenberg uncertainty principle. Let us consider the term $W^{(1)}(p,q,t)$ in more detail. It was first proposed in [11]. Later on it was demonstrated that the multiple integral (2.23) can be calculated stochastically by Monte Carlo techniques [12, 13, 14]. For this we need to generate an ensemble of trajectories in phase space. To each trajectory we ascribe a specific weight, which gives its contribution to (2.23). For example, let us consider a trajectory which starts at point $\{p_0, q_0, \tau = 0\}$. This trajectory acquires a weight equal to the value $W_0(p_0, q_0)$. Up to the time $\tau = t_1$ the trajectory is defined by the Green function $G(p_1 - s_1, q_1, t_1; p_0, q_0, 0)$. At $\tau = t_1$, as it follows from (2.23), the weight of this trajectory must be multiplied by the factor $\omega(s_1, q_1, t_1)$, and simultaneously a perturbation in momentum takes place: $(p_1 - s_1) \rightarrow p_1$. As a result the trajectory becomes discontinuous in momentum space, but continuous in the coordinate space. Obviously this is a manifestation of the Heisenberg uncertainty of coordinates and momenta. Now the trajectory consists of two parts – two classical trajectories which are the solutions of (2.19), which are separated, at $\tau = t_1$ by a momentum jump of magnitude s_1. What about the value s_1 of the jump and the time moment t_1? Both appear under integrals with a certain probability. To sample this probability adequately, a statistical ensemble of trajectories should be generated, further the point in time t_1 must be chosen randomly in the interval $[0,t]$, and the momentum jump s_1 randomly in the interval $[-\infty, +\infty]$. Finally, also different starting points $\{p_0, q_0\}$ of trajectories at $\tau = 0$ must be considered due to the integration $\int \mathrm{d}p_0 \mathrm{d}q_0$. Considering a sufficiently large

number of trajectories of such type we can accurately calculate $W^{(1)}(p,q,t)$ – the first correction to the classical evolution of the quantum distribution function $W^{(0)}(p,q,t)$.

Let us now take into account the third term in (2.22). We substitute, instead of $W(p_2 - s_2, q_2, t_2)$, its integral representation, using (2.21). As a result we get for this term

$$W^{(2)}(p,q,t) = \int\limits_0^t dt_1 \int d1 G(p,q,t;1,t_1) \int\limits_{-\infty}^{\infty} ds_1 \, \omega(s_1, q_1, t_1)$$

$$\times \int\limits_0^{t_1} dt_2 \int d2 \, G(p_1 - s_1, q_1, t_1; 2, t_2) \int\limits_{-\infty}^{\infty} ds_2 \, \omega(s_2, q_2, t_2)$$

$$\times \int d0 G(p_2 - s_2, q_2, t_2; 0, 0) \, W_0(0) \, . \tag{2.24}$$

If we apply the stochastic interpretation of the integrals, as we did above for $W^{(1)}(p,q,t)$, this term can be analogously calculated using an ensemble of classical trajectories with *two* momentum jumps taking place at time moments $\tau = t_1$ and $\tau = t_2$, and with a weight function multiplied by the factors $\omega(s_1, q_1, t_1)$ and $\omega(s_2, q_2, t_2)$, respectively.

Applying the above procedure several times, we can get the higher order correction terms. As a result, $W(p,q,t)$ will be expressed as an iteration series, with each term of the series representing a contribution of trajectories of a definite topological type – with one, two, three, etc. momentum jumps. In Fig. 2.7 we show an example of trajectories contributing to the terms $W^{(0)}$, $W^{(1)}$ and $W^{(2)}$.
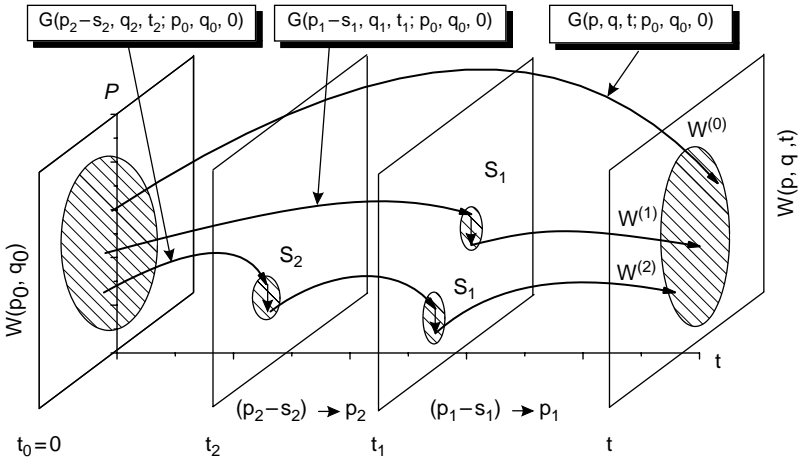

Fig. 2.7. Illustration of the iteration series. Three types of trajectories are shown: Without (*top curve*), with one (*middle*) and with two (*lower*) momentum jumps

As was noted in Sect. 2.1 the Wigner function allows us to compute the quantum-mechanical expectation value of an arbitrary one-particle operator $\widehat{A}$. Using the idea of iteration series (2.22), we obtain an iteration series also for the expectation value

$$\langle \widehat{A}\rangle(t) = \int \mathrm{d}p\mathrm{d}q\ A(p,q)W(p,q,t) = \langle \widehat{A}\rangle^{(0)}(t) + \langle \widehat{A}\rangle^{(1)}(t) + \dots\ , \qquad (2.25)$$

where different terms correspond to different terms in the series for W. The series (2.25) maybe computed much more efficiently than the one for W since the result does not depend on coordinates and momenta anymore.

Certainly, in the iteration series it is possible to take into account only a finite number of terms and contributions of a limited number of trajectories. Interestingly, it is not necessary to compute the individual terms iteratively. Instead, all relevant terms can be calculated simultaneously using the basic concepts of MC methods [26]. An important task of the MC procedure will be to generate stochastically the trajectories which give the dominant contribution to the result, for details see [10].

2.4 Time Correlation Functions in the Canonical Ensemble

So far we have considered the dynamics of pure states where the density matrix ρ, which is the matrix representation of the density operator $\widehat{\rho}$, is defined by a single wave function ψ. However, at finite temperature ρ is, in general, defined by an incoherent superposition of wave functions (mixed states). Here we consider the canonical ensemble as the most common one. Time correlation functions $C_{FA}(t) = \langle F(0)A(t)\rangle$ are among the most important quantities in statistical physics which describe transport properties, such as diffusion, dielectric properties, chemical reaction rates, equilibrium or non-equilibrium optical properties. An example has already been considered in Sect. 2.2 – the density-density auto-correlation function (2.13). Here we use a more general expression for the quantum correlation function of two quantities A and F given by the operators $\widehat{F}$ and $\widehat{A}$. In the canonical ensemble the averaging is performed by a trace with the canonical density operator $\widehat{\rho}^{\mathrm{eq}} = Z^{-1}\exp(-\beta\widehat{H})$, with $\beta = 1/k_{\mathrm{B}}T$, and the correlation function has the form [27]

$$C_{FA}(t) = \frac{1}{Z}\mathrm{Tr}\left(\widehat{F}\ \mathrm{e}^{\mathrm{i}\widehat{H}t_{\beta}^{*}}\ \widehat{A}\ \mathrm{e}^{-\mathrm{i}\widehat{H}t_{\beta}}\right)\ , \qquad (2.26)$$

where $\widehat{H}$ is the Hamiltonian (2.3), t_{β} is a complex time argument $t_{\beta} = t - \mathrm{i}\beta/2$ which absorbs $\widehat{\rho}^{\mathrm{eq}}$, $Z = \mathrm{Tr}\widehat{\rho}^{\mathrm{eq}}$ is the partition function, and we use $\hbar = 1$.

The time correlation function can now be computed by first writing (2.26) in coordinate representation and then transforming to the Wigner picture, using the Weyl representation of $\widehat{F}$ and $\widehat{A}$,

$$C_{FA}(t) = \frac{1}{Z} \int dq_1 dq_2 dq_3 dq_4 \left\langle q_1 | \widehat{F} | q_2 \right\rangle \left\langle q_2 | e^{i\widehat{H}t_\beta^*} | q_3 \right\rangle$$

$$\times \left\langle q_3 | \widehat{A} | q_4 \right\rangle \left\langle q_4 | e^{-i\widehat{H}t_\beta} | q_1 \right\rangle$$

$$= \int dp_1 dq_1 dp_2 dq_2 \; F(p_1, q_1) \; A(p_2, q_2) \; W(p_1, q_1; p_2, q_2; t; \beta) \; ,$$

(2.27)

where $W(p_1, q_1; p_2, q_2; t; \beta)$ is now a generalization of the Wigner function which is defined as double Fourier transformation of the product of two non-diagonal matrix elements of the density operator

$$W(p_1, q_1; p_2, q_2; t; \beta) = \frac{1}{Z(2\pi)^{2Nd}} \int d\xi_1 d\xi_2 \; e^{ip_1 \xi_1} \; e^{ip_2 \xi_2}$$

$$\times \left\langle q_1 - \frac{\xi_1}{2} \left| e^{i\widehat{H}t_\beta^*} \right| q_2 + \frac{\xi_2}{2} \right\rangle \left\langle q_2 - \frac{\xi_2}{2} \left| e^{-i\widehat{H}t_\beta} \right| q_1 + \frac{\xi_1}{2} \right\rangle . \quad (2.28)$$

Calculating the partial time derivatives of the function W it can be shown that the function W satisfies a system of two Wigner-Liouville equations [12, 13]

$$\frac{\partial W}{\partial t} + \frac{p_1}{m} \cdot \nabla_{q_1} W + F(q_1) \cdot \nabla_{p_1} W = I_1 \; ,$$

$$\frac{\partial W}{\partial t} + \frac{p_2}{m} \cdot \nabla_{q_2} W + F(q_2) \cdot \nabla_{p_2} W = I_2 \; ,$$

(2.29)

where on the r.h.s. we have two collision integrals

$$I_1 = \int_{-\infty}^{\infty} ds_1 \; W(p_1 - s_1, q_1; p_2, q_2; t; \beta) \; \omega(s_1, q_1, t) \; ,$$

$$I_2 = \int_{-\infty}^{\infty} ds_2 \; W(p_1, q_1; p_2 - s_2, q_2; t; \beta) \; \omega(s_2, q_2, t) \; , \quad (2.30)$$

and the function $\omega(s, q, t)$ is defined in the same way as in the microcanonical ensemble, see (2.16).

2.4.1 Initial Conditions for the Wigner-Liouville Equation

Using (2.28) at $t = 0$, we find that the initial value of the Wigner function is given by the integral

$$W_0(1; 2; 0; \beta) = \frac{1}{Z(2\pi)^{2Nd}} \int d\xi_1 d\xi_2 \; e^{ip_1 \xi_1} \; e^{ip_2 \xi_2}$$

$$\times \left\langle q_1 - \frac{\xi_1}{2} \left| e^{-\beta\widehat{H}/2} \right| q_2 + \frac{\xi_2}{2} \right\rangle \left\langle q_2 - \frac{\xi_2}{2} \left| e^{-\beta\widehat{H}/2} \right| q_1 + \frac{\xi_1}{2} \right\rangle \quad (2.31)$$

with $1 = q_1, p_1$ and $2 = q_2, p_2$.

Let us now exploit the group property of the density operator $\widehat{\rho}$ and the high temperature approximation for the matrix elements of $\langle q'|\widehat{\rho}|q\rangle$ (see Chap. 13)

$$\mathrm{e}^{-\beta\widehat{H}} = \left[\mathrm{e}^{-\beta/M\widehat{H}}\right]^M$$

$$\left\langle q'\left|\mathrm{e}^{-\beta/(2M)\widehat{H}}\right|q''\right\rangle \approx \left\langle q'\left|\mathrm{e}^{-\beta/(2M)\widehat{K}}\right|q''\right\rangle \left\langle q'\left|\mathrm{e}^{-\beta/(2M)\widehat{U}}\right|q''\right\rangle . \quad (2.32)$$

Then we obtain

$$W_0(1;2;0;\beta) \approx \frac{1}{Z(2\pi\hbar)^{2Nd}} \int \mathrm{d}q_1' \ldots \mathrm{d}q_M' \, \mathrm{d}q_1'' \ldots \mathrm{d}q_M'' \mathrm{e}^{-\sum_{m=2}^{M} K_m - \sum_{m=1}^{M} U_m}$$

$$\times \int \mathrm{d}\xi_1 \mathrm{e}^{\mathrm{i}p_1\xi_1/\hbar} \left\langle q_M'\left|\mathrm{e}^{-\beta\widehat{K}/(2M)}\right|q_1+\frac{\xi_1}{2}\right\rangle \left\langle q_1-\frac{\xi_1}{2}\left|\mathrm{e}^{-\beta\widehat{K}/(2M)}\right|q_1''\right\rangle$$

$$\times \int \mathrm{d}\xi_2 \mathrm{e}^{\mathrm{i}p_2\xi_2/\hbar} \left\langle q_M''\left|\mathrm{e}^{-\beta\widehat{K}/(2M)}\right|q_2+\frac{\xi_2}{2}\right\rangle \left\langle q_2-\frac{\xi_2}{2}\left|\mathrm{e}^{-\beta\widehat{K}/(2M)}\right|q_1'\right\rangle ,$$
$$(2.33)$$

where $K_m = (\pi/\lambda_M^2)\left[(q_m'-q_{m-1}')^2 + (q_m''-q_{m-1}'')^2\right]$ and $U_m = (\beta/(2M)) [U(q_m') + U(q_m'')]$. Here we have assumed that $M \gg 1$, and $\lambda_M^2 = 2\pi\hbar^2\beta/(mM)$ denotes the thermal de Broglie wave length corresponding to the inverse temperature $\beta/(2M)$. A direct calculation of the last two factors in (2.33) gives

$$\int \mathrm{d}\xi_1 \mathrm{e}^{\mathrm{i}p_1\xi_1/\hbar} \left\langle q_M'\left|\mathrm{e}^{-\beta\widehat{K}/(2M)}\right|q_1+\frac{\xi_1}{2}\right\rangle \left\langle q_1-\frac{\xi_1}{2}\left|\mathrm{e}^{-\beta\widehat{K}/(2M)}\right|q_1''\right\rangle$$

$$= \left\langle q_M'\left|\mathrm{e}^{-\beta\widehat{K}/(2M)}\right|q\right\rangle \phi(p;q_M',q_1) \left\langle q\left|\mathrm{e}^{-\beta\widehat{K}/(2M)}\right|q_1\right\rangle , \quad (2.34)$$

where

$$\phi\left(p;q_M',q_1\right) = (2\lambda_M^2)^{Nd/2}\mathrm{e}^{-(p\lambda_M/\hbar+\mathrm{i}\pi(q'-q'')/\lambda_M)^2/(2\pi)} \quad (2.35)$$

The final result for the Wigner function at $t = 0$ can be written as

$$W(1;2;0;\beta) \approx \int \mathrm{d}q_1' \ldots \mathrm{d}q_M' \, \mathrm{d}q_1'' \ldots \mathrm{d}q_M'' \, \Psi(1;2;q_1' \ldots q_M';q_1'' \ldots q_M'';0;\beta)$$

$$\times \phi(p_2;q_M',q_1'') \, \phi(p_1;q_M'',q_1') , \quad (2.36)$$

where

$$\Psi(p_1,q_1;p_2,q_2;q_1' \ldots q_M';q_1'' \ldots q_M'';\beta) = \frac{1}{Z}\mathrm{e}^{-\sum_{m=1}^{M+1} K_m - \sum_{m=1}^{M} U_m} . \quad (2.37)$$

Here we have introduced the notation $\{q_0' \equiv q_1; q_0'' \equiv q_2\}$ and $\{q_{M+1}' \equiv q_2; q_{M+1}'' \equiv q_1\}$. Fig. 2.8 illustrates the simulation idea. Two closed loops with the set of points
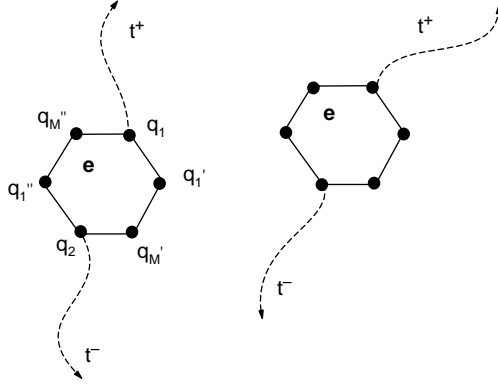
Fig. 2.8. Two closed loops illustrating the path integral representation of two electrons in the density matrices in (2.33). Two special points, (p_1, q_1) and (p_2, q_2), are starting points for two dynamical trajectories propagating forward and backward in time

show the path integral representation of the density matrices in (2.33). The left chain of points, i.e. $\{q_1, q_1', \ldots, q_M', q_2, q_1'', \ldots, q_M''\}$ characterizes the path of a single quantum particle. The chain has two special points (p_1, q_1) and (p_2, q_2). As it follows from (2.28) and (2.29) these points are the original points for the Wigner function, the additional arguments arise from the path integral representation. As we show in the next section, we can consider these points as starting points for two dynamical trajectories propagating forward and backward in time, i.e. $t \to t^+$ and $t \to t^-$. The Hamilton equations for the trajectories are defined in the next section.

2.4.2 Integral Equations

The solution follows the scheme explained before. The only difference is that we now have to propagate two trajectories instead of one,

$$\frac{d\bar{q}_1}{d\tau} = \frac{\bar{p}_1(\tau)}{2m} \;, \qquad \bar{q}_1(0) = q_1^0 \;,$$

$$\frac{d\bar{p}_1}{d\tau} = \frac{1}{2}\boldsymbol{F}[\bar{q}_1(\tau)] \;, \qquad \bar{p}_1(0) = p_1^0 \;,$$

$$\frac{d\bar{q}_2}{d\tau} = -\frac{\bar{p}_2(\tau)}{2m} \;, \qquad \bar{q}_2(0) = q_2^0 \;,$$

$$\frac{d\bar{p}_2}{d\tau} = -\frac{1}{2}\boldsymbol{F}[\bar{q}_2(\tau)], \qquad \bar{p}_2(0) = p_2^0 \;. \tag{2.38}$$

The first (second) trajectory propagates forward (backward). Let us substitute expressions for $\boldsymbol{F}[\bar{q}_1(\tau)], \bar{p}_1(\tau), \boldsymbol{F}[\bar{q}_2(\tau)]$ and $\bar{p}_2(\tau)$ from (2.38) into (2.29) and subtract the second equation from the first. As a result, on the l.h.s. we obtain a full differential of the Wigner function. After multiplication by the factor $1/2$ and integration over time, the integral equation for the Wigner function takes the form

$$W(p_1, q_1; p_2, q_2; t; \beta) = \int \mathrm{d}p_1^0 \mathrm{d}q_1^0 \mathrm{d}p_2^0 \mathrm{d}q_2^0$$

$$\times G(p_1, q_1, p_2, q_2, t; p_1^0, q_1^0, p_2^0, q_2^0, 0) W(p_1^0, q_1^0; p_2^0, q_2^0; 0; \beta)$$

$$+ \int_0^t \mathrm{d}\tau \int \mathrm{d}p_1^1 \mathrm{d}q_1^1 \, \mathrm{d}p_2^1 \mathrm{d}q_2^1 \, G(p_1, q_1, p_2, q_2, t; p_1^1, q_1^1, p_2^1, q_2^1, \tau)$$

$$\times \int_{-\infty}^{\infty} \mathrm{d}s \, \mathrm{d}\eta \, \vartheta(s, q_1^1; \eta, q_2^1; \tau) \, W(p_1^1 - s, q_1^1; p_2^1 - \eta, q_2^1; \tau; \beta) , \qquad (2.39)$$

where $\vartheta(s, q_1^1; \eta, q_2^1; \tau) = [\omega(s, q_1^1)\delta(\eta) - \omega(\eta, q_2^1)\delta(s)]/2$. The dynamical Green function G is defined as $G(p_1, q_1, p_2, q_2, t; p_1^0, q_1^0, p_2^0, q_2^0, 0) = \delta[p_1 - \bar{p}_1(\tau; p_1^0, q_1^0, 0)]$ $\delta[q_1 - \bar{q}_1(\tau; p_1^0, q_1^0, 0)]\delta[p_2 - \bar{p}_2(\tau; p_2^0, q_2^0, 0)]\delta[q_2 - \bar{q}_2(\tau; p_2^0, q_2^0, 0)]$. Let us denote the first term on the r.h.s. of (2.39) as $W^{(0)}(p_1, q_1; p_2, q_2; t; \beta)$. This term represents the Wigner function of the initial state propagating along classical trajectories (characteristics – solutions of (2.38)). Using the approach applied for the microcanonical ensemble, we obtain expressions for $W^{(1)}(p_1, q_1; p_2, q_2; t; \beta)$, $W^{(2)}(p_1, q_1; p_2, q_2; t; \beta), \dots$ and represent $W(p_1, q_1; p_2, q_2; t; \beta)$ as iteration series. In this case, we can calculate this also with an ensemble of trajectories using the quantum dynamics MC approach described in [28]. As a result the expression for the time correlation function (2.27) can be rewritten as

$$C_{FA}(t) = \int \mathrm{d}p_1 \mathrm{d}q_1 \, \mathrm{d}p_2 \mathrm{d}q_2 F(p_1, q_1) A(p_2, q_2) W(p_1, q_1; p_2, q_2; t; \beta)$$

$$= \left(\phi(P) | W^{(0)}(P; \beta) \right) + \sum_{i=1}^{\infty} \left(\phi(P) | W^{(i)}(P; \beta) \right) , \qquad (2.40)$$

where $\left(\phi(P) | W^{(i)}(P; \beta) \right)$ denotes the integral in the phase space $\{p_1, q_1, p_2, q_2\}$ (now we consider a $2N$-particle system), and $\phi(P) = F(p_1, q_1) A(p_2, q_2)$.

An illustrative example for the calculations of the time correlation functions C_{FA} is the momentum-momentum autocorrelation function $C_{PP}(t)$ for a 1D system of interacting electrons in an array of fixed random scatterers at finite temperature [28]. This system is of high interest because at zero temperature it shows Anderson localization if e-e interaction is neglected. It is a long standing question what the effect of e-e interaction on localization will be. The present method is, in principle, well suited to answer this question. In [28] the first applications of the method to an 1D system at finite temperature have been presented showing that Coulomb e-e interaction has the trend to enhance the mobility of localized electrons [10, 28].

2.5 Discussion

We have presented a general idea how to extend the powerful method of molecular dynamics to quantum systems. First, we discussed semi-classical MD, i.e., classical

MD with accurate quantum pair potentials. This method is very efficient and allows to compute thermodynamic properties of partially ionized plasmas for temperatures above the molecule binding energy (i.e. as long as three and four particle correlations can be neglected). Further, frequency dependent quantities, e.g., the plasmon spectrum, are computed correctly for $\omega < \omega_{pl}$. Further progress is possible if more general quantum potentials are derived.

In the second part, we considered methods for a rigorous solution of the quantum Wigner-Liouville equation for the N-particle Wigner function. Results were derived for both, a pure quantum state and a mixed state (canonical ensemble). Although this method is by now well formulated, it is still very costly in terms of CPU time, so that practical applications are only starting to emerge. Yet, we expect that, due to its first principle character, Wigner function QMD will become increasingly important for a large variety of complex many-body problems.

References

1. M. Allen, D. Tildesley, *Computer Simulations of Liquids* (Clarendon Press, Oxford, 1987)
2. D. Frenkel, B. Smit, *Understanding Molecular Simulations: From Algorithms to Applications* (Academic Press, Fribourg, 2002)
3. H. Feldmeier, J. Schnack, Rev. Mod. Phys. **72**, 655 (2000)
4. D. Klakow, C. Toepffer, P.G. Reinhard, Phys. Lett. A **192**, 55 (1994)
5. D. Klakow, C. Toepffer, P.G. Reinhard, J. Chem. Phys. **101**(12), 10766 (1994)
6. G. Zwicknagel, T. Pschiwul, J. Phys. A: Math. General **39**, 4359 (2006)
7. M. Bonitz, *Quantum Kinetic Theory* (B.G. Teubner, Stuttgart/Leipzig, 1998)
8. E. Wigner, Phys. Rev. **40**, 749 (1932)
9. V. Tatarsky, Sov. Phys. Usp. **26**(4), 311 (1983)
10. M. Bonitz, D. Semkat (eds.), *Introduction to Computational Methods in Many Body Physics* (Princeton: Rinton Press, 2006)
11. V. Filinov, Y. Medvedev, V. Kamskyi, Mol. Phys. **85**(4), 711 (1995)
12. V. Filinov, Mol. Phys. **88**(6), 1517 (1996)
13. V. Filinov, Y. Lozovik, A. Filinov, E. Zakharov, A. Oparin, Phys. Scripta **58**, 297 (1998)
14. Y. Lozovik, A. Filinov, Sov. Phys. JETP - USSR **88**, 1026 (1999)
15. Y. Lozovik, A. Filinov, A. Arkhipov, Phys. Rev. E **67**, 026707 (2003)
16. G. Kelbg, Ann. Physik **467**(3–4), 219 (1963)
17. G. Kelbg, Ann. Physik **467**(7–8), 354 (1964)
18. G. Kelbg, Ann. Physik **469**(7–8), 394 (1964)
19. A. Filinov, V. Golubnychiy, M. Bonitz, W. Ebeling, J. Dufty, Phys. Rev. E **70**, 046411 (2004); W. Ebeling, A. Filinov, M. Bonitz, V. Filinov, T. Pohl, J. Phys. A: Math. Gen. **39**, 4309 (2006)

20. J. Hansen, I. McDonald, Phys. Rev. A **23**, 2041 (1981)

21. V. Filinov, M. Bonitz, W. Ebeling, V. Fortov, Plasma Phys. Contr. Fusion **43**, 743 (2001); V.S. Filinov, V.E. Fortov, M. Bonitz, D. Kremp, Physics Lett. A **274**, 228 (2000); V.S. Filinov, V.E. Fortov, M. Bonitz, P.R. Levashov, JETP Letters **74**, 384 (2001) [Pis'ma V ZhETF **74**, 422 (2001)]; M. Bonitz, V.S Filinov, VE. Fortov, P.R. Levashov, H. Fehske, Phys. Rev. Lett. **95**, 235006 (2005)

22. V. Golubnychiy, M. Bonitz, D. Kremp, M. Schlanges, Phys. Rev. E **64**, 016409 (2001)

23. H. Wagenknecht, W. Ebeling, A. Förster, Contrib. Plasma Phys. **41**, 15 (2001)

24. V. Golubnychiy, Molecular dynamics simulations of strongly correlated mesoscopic and macroscopic coulomb systems. Ph.D. thesis, Kiel University (2004)

25. M. Bonitz, A. Filinov, V. Golubnychiy, T. Bornath, W. Kraeft, Contrib. Plasma Phys. **5–6**, 450 (2005)

26. I. Sobol, *The Monte Carlo Method (Popular Lectures in Mathematics)* (University of Chicago Press, 1975)

27. D. Zubarev, *Nonequilibrium Statistical Thermodynamics* (Plenum Press, New York/London, 1974)

28. V. Filinov, P. Thomas, I. Varga, T. Meier, M. Bonitz, V. Fortov, S. Koch, Phys. Rev. B **65**, 165124 (2002)